Journal of Materials Chemistry A

Accepted Manuscript

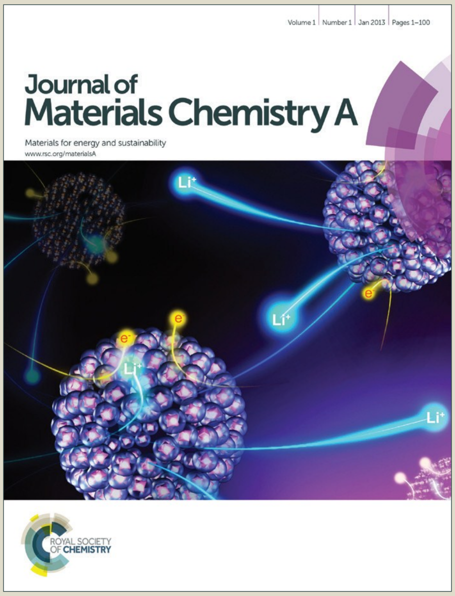

ROYAL SOCIETY OF CHEMISTRY

www.rsc.org/materialsA

Development of Pervaporation Membranes Using Chitosan and Titanium glycine-N,N-dimethylphosphonate for Dehydration of Isopropanol

H. G. Premakshi, A. M. Sajjan, M. Y. Kariduraganavar*
Department of Chemistry, Karnatak University, Dharwad 580 003, India.

Titanium glycine-N,N-dimethylphosphonate, $Ti[(O_3PCH_2)_2NCH_2COOH]$ (TGDMP), was synthesized and incorporated into chitosan in different weight ratios to obtain nanocomposite membranes. TGDMP acts as electronegative nanofiller owing to large number of –COOH groups and thereby establishes an electrostatic interaction between nanofiller and chitosan. The structure, morphology, and thermal properties of the resulting membranes were studied using different techniques such as Fourier transform infrared (FTIR) spectroscopy, wide-angle X-ray diffraction (WAXD), differential scanning calorimetry (DSC), thermogravimetric analysis (TGA) and scanning electron microscopy (SEM). The membranes were subjected to pervaporation dehydration of isopropanol at different temperatures. The effect of TGDMP on the pervaporation performance was investigated systematically. The separation factor and permeation flux of the resulting nanocomposite membranes are much higher than that of the pure chitosan membrane. The membrane containing 1.2 mass% of TGDMP demonstrated the highest separation factor of 1,050 with a permeation flux of 7.37×10^{-2} kg/m^{2}h at 30 ºC for 10 mass% of water in the feed. The total flux and flux of water are found to be overlapping particularly for TGDMP incorporated membranes, illustrating that the developed nanocomposite membranes could be used effectively to break the azeotropic point of water-isopropanol mixtures. From the temperature dependent diffusion and permeation values, the Arrhenius activation parameters were estimated. The activation energy values obtained for water permeation (E_{pw}) are significantly lower than those of isopropanol permeation (E_{pIPA}), suggesting that the developed membranes have a higher separation ability for the water-isopropanol system. The estimated E_p and E_D values ranged between 20.00 and 2.52, and 19.72 and 2.48 kJ/mol, respectively. A positive heat of sorption (ΔH_S) values was obtained for all the membranes, suggesting that Henry's mode of sorption was predominant.

Keywords: Chitosan; Titanium glycine-N,N-dimethylphosphonate; Pervaporation; Separation factor; Activation energy.

---

*Corresponding author: Dr. M. Y. Kariduraganavar (mahadevappayk@gmail.com) Fax: +91-836-2771275; Phone: +91-836-2215286 (Extn. 23).

1. Introduction

To solve the problems associated with energy security and global warming, there is an urgent need to explore and develop both energy saving and environmental friendly processes for chemical industries.[1,2] The literature clearly indicates that typically, in chemical processes, separation accounts for 60-80% of the process cost.[3] Of course, distillation, gas stripping and molecular sieve adsorption are conventional methods, and have been employed for the dehydration of alcohols, but these processes often have intensive energy demands and large footprints. To overcome this, pervaporation (PV) offers an alternative economic and eco-friendly technique. Therefore, it is being considered as a potential process for the dehydration of alcohols.[4,5]

Substantial work has been undertaken in the past to explore high performance PV membranes for the separation of alcohol-water mixtures. Many studies reveal that ideal PV membranes must have excellent permeability, separation factor and durability to demonstrate commercial viability.[6-8] Generally, hydrophilic polymer membranes have attracted considerable interest owing to their strong affinity towards water, which leads to high separation factor and good flux. Among the hydrophilic polymers, chitosan (CS), a cationic deacetylated polysaccharide obtained from chitin, is a promising membrane material for the dehydration of isopropanol. Owing to its good biocompatibility, biodegradability, low cost and the presence of multiple functional groups, it has been used in various fields including waste-water treatment,[9] membrane separation,[10] wound dressing[11] and food packaging.[12] However, the poor mechanical properties, low thermal stability and high hydrophilicity of chitosan restrict its range of potential applications. Many researchers have tried to overcome this by blending,[13] crosslinking,[14] grafting[15] or by introducing fillers like zeolites,[16,17] silver nanoparticles,[18] clay materials, silica,[6] etc. All these have proved to be effective ways to improve the mechanical and thermal properties of membranes. However, the transport properties of the membranes, particularly in the field of pervaporation, still require enhancement. Pure chitosan membranes are inexpensive and easy to fabricate, but usually there is a trade-off phenomenon between flux and separation factor. Very recently reports have indicated that P-OH groups anchored to a surface layer of zirconium phosphate can be replaced with P–OR or P–R groups (R is an organic group) without altering the inorganic texture of the layers,[19] providing a new approach for modifying the polymers. Accordingly, Wu et al.[20] and Cascicia et al.[21] respectively developed nanocomposite membranes with starch/zirconium phosphonate and polyvinylidene fluoride/ZrSPP. Similarly, chitosan/ZrSP and epoxy/layered zirconium phosphonate (Zr-P) nanocomposite membranes were synthesized by Yang et al.[22] and Tsai et al.,[23] respectively. All these membranes demonstrated an excellent PV performance in addition to good mechanical and thermal properties. This prompted us to modify the chitosan membrane by incorporating titanium glycine-N,N-dimethylphosphonate as nanofiller for the enhancement of the overall PV performance.

In the present study TGDMP was synthesized and incorporated into chitosan in different weight ratios so as to obtain nanocomposite membranes. TGDMP is electronegative nanofiller owing to the large number of -COOH groups. These groups enhance the electrostatic interaction between the nanofiller and chitosan, and would be expected to improve the overall performance of membranes. The physico-chemical properties of the resulting membranes have been studied using different techniques and the membranes successfully employed for the PV separation of water-isopropanol mixtures at different temperatures. The values of permeation flux and separation factor were determined systematically and the diffusion coefficient and Arrhenius activation parameters have also been estimated. The results are discussed in terms of the PV separation efficiency of the membranes.

2. Experimental section

Chitosan ($\bar{M}_w$ ~ 200,000; *N*-deacetylation degree 75-85%) was procured from Sigma-Aldrich Chemicals, USA. Titanium chloride ($TiCl_4$) and phosphorus oxide were purchased from Spectrochem Pvt. Ltd., Mumbai, India. *N,N*-Bis(phosphonomethyl)-glycine ($(H_2O_3PCH_2)_2NCH_2COOH$) was synthesized according to the procedure developed by Li et al.[24] Hydrochloric acid, isopropanol (IPA), acetic acid and other reagents were purchased from s. d. fine Chemicals Ltd., Mumbai, India. All the chemicals were of reagent grade and used without further purification. Double distilled water was used throughout the study.

Preparation of titanium glycine-N,N-dimethylphosphonate (TGDMP)

TGDMP was synthesized according to the procedure reported by Li et al.[24] Hydrochloric acid (2 M; 430 ml) containing 0.3 M $TiCl_4$ was slowly added into a solution of *N,N*-bis(phosphonomethyl)-glycine (0.63 M; 400 ml). After 24 h, the precipitate thus obtained was filtered and washed with distilled water until the pH of the filtrate was around 3 to 3.5, and it was then dried over P_2O_5 (see ESI-Figure S1).

Membrane preparation

Chitosan (3 g) was dissolved at room temperature in 100 ml of deaerated distilled water containing 2% of acetic acid with constant stirring for about 24 h. The solution was then filtered and the resulting homogeneous solution was spread onto a clean glass plate with the aid of a casting knife in a dust-free atmosphere. It was then allowed to dry at ambient temperature for about 2-3 days. The completely dried membrane was subsequently peeled-off and was designated as M.

To prepare the TGDMP incorporated chitosan membrane, a known amount of TGDMP was added into a homogeneous chitosan (CS) solution. The mixture was stirred at 60 ^{o}C for 3 h. After degassing under vacuum, the CS/TGDMP solution was poured onto a glass plate and heated at around 50 ^{o}C to obtain a dry film. The rest of the procedure was followed as in the preparation of membrane M. However, the amount of TGDMP with respect to CS was varied as 0.4, 0.8, 1.2 and 1.6 mass%, and the resulting membranes were designated as M-1, M-2, M-3 and M-4, respectively. The thickness of these membranes was measured at different points using a Peacock dial thickness gauge (Model G, Ozaki MFG Co. Ltd., Japan) with an accuracy of ± 2 μm. The thickness of the membranes was found to be 40 ± 2 μm.

The interaction between CS and TGDMP was confirmed by FTIR spectroscopy (Nicolet, Impact-410, USA). Membrane samples were ground well to make KBr pellets under a hydraulic pressure of 400 kg/cm^2 and the spectra were recorded in the range 400-4000 cm^{-1}. In each scan, the amount of membrane sample and KBr were kept constant in order to know the changes in the intensities of the characteristic peaks with respect to the amount of TGDMP.

The crystallinity of the plain CS and its nanocomposite membranes was studied at room temperature using a Philips analytical X-ray diffractometer. The X-ray source was nickel-filtered Cu-Kα radiation (40 kV, 30 mA). The dried membranes of uniform thickness (~ 40 μm) were mounted on a sample holder and scanned in the reflection mode at an angle 2θ over a range from 5 to 50^o at a speed of 8^o/min.

The glass transition temperatures of pure CS and its nanocomposite membranes were measured using a differential scanning calorimeter (DSC Q 20, TA Instruments, Waters LLC, USA) at a heating rate of 10 ºC/min under a nitrogen atmosphere. The weight of the samples taken for each record was 6-9 mg. The thermal properties of pure CS and its nanocomposite membranes were also studied using a thermogravimetric analyzer (DSC Q 20, TA Instruments, Waters LLC, USA) at a heating rate of 10 ºC/min under nitrogen atmosphere. The weight of the samples taken for each run was 6-9 mg.

The surface and cross-section views of pure CS and its nanocomposite membranes were examined using a scanning electron microscope (JEOL, JSM-400 Å, Tokyo, Japan). Before photographing, all the samples were dried in vacuum and coated with a conductive layer (400 Å) of sputtered gold.

Swelling measurement

Equilibrium sorption experiments for the membranes were performed in different compositions of water-IPA mixtures using an electronically controlled oven (WTB Binder, Jena, Germany). The masses of the dry membranes were first determined and were equilibrated by soaking in different compositions of water-IPA mixtures in sealed vessels at 30 ºC for 24 h. The swollen membranes were removed and weighed as quickly as possible (after careful blotting) on a digital microbalance (Mettler, B204-S, Toledo, Switzerland) within an accuracy of ± 0.01 mg. The percent degree of swelling (*DS*) was calculated as:

$$DS\,(\%) = \left(\frac{W_s - W_d}{W_d}\right) \times 100 \qquad (1)$$

where W_s and W_d are the masses of the swollen and dry membranes, respectively.

Pervaporation experiments

The PV experiments were performed using an indigenously designed apparatus as reported in our previous articles.[25,26] The effective surface area of the membrane in contact with the feed mixture was 34.23 cm^2 and the capacity of the feed compartment was about 250 cm^3. The vacuum in the downstream side of the apparatus was maintained [1.333224×10^3 Pa (10 Torr)] using a two-stage vacuum pump (Toshniwal Instruments, Chennai, India). The water composition in the feed mixture was varied from 5 to 25 mass%. Before performing the PV experiment, the test membrane was allowed to equilibrate with a known volume of feed mixture for about 2 h in the feed compartment. After a steady state was attained, the permeate was collected in a trap, immersed in liquid nitrogen, on the downstream side at a fixed intervals of time. The experiments were carried out at 30, 40 and 50 ºC. The flux was calculated by weighing the permeate on a digital microbalance with an accuracy of ± 0.01 mg. The compositions of water and isopropanol were estimated by measuring the refractive index of the permeate within an accuracy of ± 0.0001 units using an Abbe refractometer (Atago-3T, Japan) and by comparing it with a standard graph, that had previously been constructed using known compositions of water-isopropanol mixtures. All the experiments were performed at least three times and the results were averaged. The results of permeation for water-IPA mixtures during the pervaporation were reproducible within an acceptable range.

From the PV data, the separation performance of the membranes was determined in terms of the total flux (*J*), separation factor (α_{sep}) and pervaporation separation index (*PSI*); these were calculated using the following equations:

$$J = \frac{W}{A.t} \tag{2}$$

$$\alpha_{sep} = \frac{P_w / P_{IPA}}{F_w / F_{IPA}} \tag{3}$$

$$PSI = J(\alpha_{\mathrm{sep}} - 1) \tag{4}$$

where W is the mass of permeate (kg); A, the effective membrane area (m^2); t, the permeation time (h); P_w and P_{IPA} are the mass percent of water and isopropanol in the permeate, respectively. F_w and F_{IPA} are the respective mass percent of water and isopropanol in the feed.

3. Results and discussion

The interaction between TGDMP and chitosan is illustrated in Figure 1. A different weight ratio of TGDMP was added to a known amount of quaternized chitosan solution at 60 ºC and stirred for 3 h. The ionized carboxylic groups of TGDMP interacted with the quaternized amino groups of chitosan. As a result, an electrostatic interaction and hydrogen bonding developed between chitosan and TGDMP, strengthening the interfacial adhesion. This could enhance the thermal and mechanical properties of the nanocomposite membranes and consequently improve the overall PV performance.

Membrane characterization

The FTIR spectra of TGDMP, pure chitosan and their nanocomposite membranes are shown in Figure 2. In the TGDMP spectrum, a broad band appeared at 3444 cm^{-1}. This was attributed to adsorbed moisture and hydrogen bonding occurring between the carboxylic groups.[27] The bands appearing at 1735 and 1638 cm^{-1} are respectively assigned to –COOH and $–COO^{-}$ stretching vibrations;[27,28] a broad band appearing in the range 1000–1200 cm^{-1} is the characteristic band of phosphate groups;[29,30] a weak band appeared at 612 cm^{-1} was attributed to the deformation vibration of Ti–O bond.[31] Taken together these bands indicate that the TGDMP was successfully synthesized.

A characteristic strong and broad band appeared at around 3390 cm^{-1} in the pure CS membrane (M). This was assigned to -OH stretching vibrations of the hydroxyl groups, which overlap with the N–H stretching vibrations.[32] The band appearing at around 2870 cm^{-1} was typical of C–H stretching vibrations. The small bands appearing at 1653 and 1538 cm^{-1} were respectively assigned to C=O stretching (amide I) and N–H bending (amide II) vibrations.[33] Upon incorporating the TGDMP in the pure CS membrane matrix, it was noticed that the characteristic bands that had appeared at 3390, 2870 and 1538 cm^{-1} in CS were shifted to 3404, 2882 and 1579 cm^{-1}, respectively. This is attributed to enhanced hydrogen bonding and electrostatic interaction between chitosan and the TGDMP. This indicates that there was good compatibility between chitosan and the TGDMP, which could lead to good PV performance.

To study the effect of TGDMP on the crystallinity of the chitosan membrane, X-ray diffraction was performed for all the membranes and the patterns thus obtained are displayed in Figure 3. In the diffraction pattern, a pure chitosan membrane exhibited sharp peaks at around 9.5° and 15°, and a broad peak at around 21°. The sharp peaks are assigned to the existence of a semicrystalline (hydrated and anhydrous crystalline) structure, while the broad peak is due to the existence of an amorphous structure.[34] Compared with the pure CS membrane, the TGDMP incorporated nanocomposite membranes showed almost similar XRD patterns apart from the intensity of the diffraction peaks at 9.5° and 15°. Unfortunately the characteristic diffraction peaks of TGDMP could not be observed in the composites, presumably due to the low loading and its poor crystallinity. With increasing the TGDMP content although the change in intensities was small, there was a marginal increase, especially for membranes M-3 and M-4. This is expected as the functional groups (-OH, NH_3^+ and NH_2) of the CS membrane underwent significant changes due to the formation of an ionic interaction and hydrogen bonding with the TGDMP as shown in Figure 1. This is in good agreement with the SEM results, in which one can observe the clear dispersion of TGDMP particles in the pure CS matrix. This indicates that the crystallinity of pure CS was reduced by the addition of TGDMP, and thereby maximizes the compatibility of nanocomposite membranes; consequently, the amorphous domain in the membrane matrix increased from membrane M-1 to M-4. This is responsible for the increase in overall PV performance, since the amorphous domain is known to favor the transport of selective permeants.[35,36]

The thermal properties of the TGDMP incorporated CS membranes can be assessed by its solid state properties such as the glass transition temperature (T_g). The DSC patterns of CS and its TGDMP incorporated membranes were recorded from ambient temperature to 400 °C and the patterns are presented in Figure 4. It is observed that the T_g of pure CS membrane is around 80 ^{o}C. However, this was gradually shifted from 80 to 100 ^{o}C with increasing amounts of TGDMP in the CS matrix. In addition, the area under the curve gradually decreased with increasing TGDMP in the CS matrix. This is mainly due to hindrance of the chain mobility of CS by the incorporation of TGDMP through hydrogen bonding and electrostatic interactions. In this way the incorporation of TGDMP in CS membranes improved the stability.

The thermal stability and degradation behavior of TGDMP incorporated chitosan membranes were investigated by TGA under nitrogen flow. From the thermograms (see ESI-Figure S2), it is observed that CS and its nanocomposite membranes exhibited degradation mainly in three stages at around 35-120, 200-350 and above 350 ºC. The first degradation stage is attributed to desorption of physically absorbed water molecules and acetic acid, which corresponds to around 18-22% weight loss. The second stage is the major degradation of pure CS and its nanocomposite membranes, which is around 36-44% weight loss. This is due to thermal decomposition of the polymeric network, which correspondingly decreased from membrane M to M-4. The third stage of decomposition which started at 350 ^{o}C and above, is attributed to decomposition of TGDMP. Although the degradation patterns of CS/TGDMP membranes closely match with the degradation of the pure chitosan membrane, the stability of the nanocomposite membranes are better than that of pure chitosan membrane. Based on this, it is concluded that the incorporation of TGDMP, albeit in small quantities, considerably increased the thermal stability of the chitosan membrane.

Figure 5 (A and B) illustrates the SEM photographs of surface and cross-section views of chitosan and its TGDMP incorporated membranes. From the surface photographs, it can be seen that the TGDMP particles were nano-scale in size and no layered structure was observed, further indicating that their features are amorphous in nature, rather than crystalline. This is supported by the WAXD patterns. In the images, some particles can be seen to be aggregated in the clusters, but their size was still less than 100 nm, which supports the proposition that the CS/TGDMP composite membranes were true nanocomposites. The cross-sectional views of CS and CS/TGDMP membranes are displayed in Figure 5B, as can be seen, the neat CS membrane exhibited a smooth and compact surface as expected. Similarly, in the CS/TGDMP membranes, the nanofillers were dispersed uniformly, and this is particularly apparent for membranes M-1 to M-3, suggesting that there is a good compatibility between TGDMP and chitosan. This could be attributed to a large number of carboxylic acid groups present on the surface of TGDMP, which easily form strong hydrogen bonding and electrostatic interactions and thereby a strong interfacial adhesion is formed between TGDMP and chitosan. However, a rough fracture surface could be seen in M-4, which is presumably due to poor dispersion and consequent aggregation of the TGDMP at higher loadings.

Swelling study

The characteristics of the sorption mechanism depend on the structure of the membrane, the affinity of the permeants towards the membrane, and the mutual interaction between the permeants.[37,38] In PV, membrane sorption plays a key role in the separation performance of the membrane, which is generally assessed by studying the membrane swelling in different feed mixtures. Figure 6 shows the swelling behavior of all the membranes in differently proportioned water-IPA mixtures at 30 ºC. It is observed that the degree of swelling was increased almost linearly for all the membranes with increasing the proportion of water in the feed. This is due to the increased interaction between water molecules and the membrane, owing to the presence of a large number of interactive hydrophilic groups (COO^-, NH_2, NH_3^+

and OH) in the membrane matrix. This is expected since water being more polar than IPA, and preferentially interacts with hydrophilic groups of the membrane, resulting in an increased degree of swelling. It was also found that the degree of swelling increased from membrane M to M-4; *i.e.* with increasing TGDMP in the CS matrix. This is because, TGDMP enhances the amorphous domain in the membrane as evidenced from X-ray data, since TGDMP is known to be electronegative nanofiller owing to the presence of a large number of –COOH groups. These could lead to hydrogen bonding and electrostatic interactions between TGDMP and CS. Further, the formation of hydrogen bonding becomes more predominant in the membrane matrix as the content of TGDMP increases. This weakens the intermolecular interaction existing in the chitosan matrix and consequently the crystallinity of the chitosan membrane was reduced while the free-volume in the matrix increased. Obviously, the change in membrane structure and increased free-volume are jointly responsible for the enhanced degree of swelling with increasing the TGDMP content in the chitosan membrane matrix.

Pervaporation study

Figure 7 demonstrates the effects of feed composition and TGDMP content on the total permeation flux for all the membranes at 30 ºC. It is found that the total permeation flux increases almost linearly with increasing water composition in the feed, in accordance with the results observed in the swelling study. This is mainly because of increased interactions between the water molecules and the membrane, since the membranes have a large number of hydrophilic groups such as COO^-, OH, NH_3^+ and NH_2. On the other hand, the permeation flux increased from membrane M to M-4 for all investigated water compositions. This is firstly because of increased interaction between the membrane and selective permeants, owing to the formation of hydrogen bonding and electrostatic interactions between the electronegative nanofiller (TGDMP) and CS. Secondly, an increase in the proportion of amorphous material in the membrane matrix also contributes to the increased flux as evidenced by the WAXD study.

In the PV process, the overall separation factor of a membrane is generally explained on the basis of interactions between the membrane and the permeating molecules, the molecular size of the permeating species and the pore diameter of the membrane.[5] Figure 8 displays the effects of water composition and TGDMP on the selectivity of all the membranes. It was observed that the separation factor of all the membranes decreased exponentially with increasing the mass% of water in the feed. This is because at higher water concentrations, the membranes swell greatly owing to the formation of a strong interaction between the membrane and the water molecules. As a result, a decrease in separation factor is obviously expected at higher concentration of water, irrespective of the amount of TGDMP in the membrane matrix.

In contrast to the above, the separation factor increased from membrane M to M-3 upon increasing the TGDMP content in the membrane. This is due to the formation of hydrogen bonding and electrostatic interactions between TGDMP and the CS. However, the separation factor collapsed for membrane M-4. This might be due to a poor dispersion and aggregations of nanofiller in the membrane matrix when the TGDMP content was increased beyond 1.2 mass%. This is consistent with the establishment of an inorganic phase in the membrane matrix as evidenced by the SEM photographs and is further illustrated by the data in Figure 9, which demonstrates the variation of flux and selectivity as a function of the TGDMP content in the membrane at 10 mass% of water in the feed. Generally, it is found that with increasing density of the membrane, either by increasing the crosslinking density or by incorporating another polymer in the membrane matrix, the permeation flux decreases and separation factor increases or vice versa. However in the present study, both permeation flux and separation factor were increased simultaneously with increasing content of TGDMP in the membrane from M to M-3. This is in contrast to the trade-off phenomenon which generally exists between the flux and separation factor in PV processes, a significant enhancement in the hydrophilicity, the establishment of hydrogen bonding and electrostatic interactions overcome this phenomenon.

The efficiency of the membranes in the PV process is generally assessed based on the permeation of individual components. Therefore, the extent of permeation of individual components was determined by plotting the total flux, and fluxes of water and IPA as a function of TGDMP content in the membranes for 10 mass% of water in the feed (Figure 10). From the plot, it is clear that the total flux and flux of water overlap with each other particularly for the TGDMP incorporated membranes (except M-4) and thereby the flux of IPA is negligibly small for all the membranes, suggesting that the membranes developed in the present study are highly selective towards water, with a tremendous improvement in the flux compared to a chitosan membrane. The same trend was not found for membrane M-4, for the reasons discussed above.

In order to understand the overall PV performance of the membrane, we have calculated the pervaporation separation index (*PSI*) for all the membranes at 30 ^{o}C for 10 mass% of water in the feed, and the values thus obtained are presented in Figure 11. It is observed that the *PSI* values increased almost linearly up to 0.8 mass% of TGDMP and then was increased significantly when the content of TGDMP was 1.2 mass%, signifying that this particular membrane showed an excellent performance for the separation of water-IPA mixtures. This is because, the incorporation of TGDMP into membrane matrix has not only enhanced the membrane hydrophilicity, but also enhanced the intermolecular hydrogen bonding and electrostatic interactions between TGDMP and the CS. These are together responsible for the enhancement of the overall PV performance of the membranes.

Diffusion coefficient

In the PV process, mass transport of binary liquid mixtures through a non-porous polymer membrane is generally described by a solution-diffusion mechanism, which occurs in three steps: sorption, diffusion and evaporation.[39] Thus, the permeation rate and separation factor are governed by the solubility and diffusivity of each component of the feed mixture to be separated. In the process, because of the establishment of fast equilibrium distribution between bulk feed and the upstream surface of a membrane, the diffusion step controls the transport of penetrants.[40-42] Therefore, it is important to estimate the diffusion coefficient, D_i of penetrating molecules in order to understand the mechanism of molecular transport.

From Fick's law of diffusion, the diffusion flux can be expressed as:[43]

$$J_i = -D_i \frac{dC_i}{dx} \qquad (5)$$

where J is the permeation flux per unit area (kg/m^2 s), D is the diffusion coefficient (m^2/ s), C is the concentration of permeant (kg/m^3), subscript i stands for water or IPA, and x is the diffusion length (m). For simplicity, it is assumed that the concentration profile along the diffusion length is linear. Thus, D_i can be calculated with the following equation:[44]

$$D_i = \frac{J_i \delta}{C_i} \qquad (6)$$

where δ is the membrane thickness. The calculated values of D_i at 30 ºC are presented in Table (see ESI-Table S3). As was found for the PV study, the diffusion coefficient of water increased significantly from membrane M to M-4, while suppressing the diffusion coefficient of IPA. This further supports the idea that the membranes developed in the present study with TGDMP have a remarkable ability for the separation of water from IPA. As discussed in the PV study, this was attributed to increased hydrophilicity and decreased crystallinity owing to the presence of TGDMP in the membrane matrix. It was also found that there was a considerable increase in diffusion coefficients of both water and IPA for all the membranes when the amount of water was increased in the feed. This is expected owing to a deterioration of the membranes' selectivity as discussed in the PV study. Despite this fact, the magnitude of the diffusion coefficients of water is quite high in comparison to that of IPA, suggesting that the membranes developed in the present study are still selective towards water molecules even at higher concentration of water in the feed.

Temperature effect

The effect of operating temperature on the PV performance for water-IPA mixtures was studied for all the membranes at 10 mass% of water in the feed, and the resulting values are presented in a Table (see ESI-Table S4). It was observed that the permeation rate increased from 30 to 50 ºC for all the membranes, while the separation factor decreased considerably. This is because, the higher temperature not only decreases the intermolecular interaction between permeants, but also decreases the intermolecular interaction within the membrane material, due to the large number of free –OH, $-COO^-$, NH_4^+ and $-NH_2$ groups on the membrane. These are responsible for dominating the plasticizing effect on the membrane. Consequently, the permeation of the diffusing and associated molecules through the membrane becomes easier, leading to an increase of total permeation flux while suppressing the separation factor. This effect prompted us to estimate the activation energies for permeation and diffusion using the Arrhenius type equation:[45]

$$X = X_o \exp\left(\frac{-E_x}{RT}\right) \tag{7}$$

where X represents permeation (*J*), or diffusion (*D*), X_o is a constant representing the pre-exponential factor J_o or D_o, E_x represents the activation energy for permeation or diffusion depending upon the transport process under consideration, and *RT* is the usual energy term. With increasing feed temperature, the vapour pressure in the feed compartment increases, but the vapour pressure at the permeate side is not affected. This results in an increase in the driving force with increasing the temperature.

The Arrhenius plots of log *J* and log *D* versus 1/T were plotted (see ESI-Figures S5 and S6) for the temperature dependence of permeation flux and diffusion, respectively. From the least squares fits of these linear plots, the activation energies for total permeation (E_p) and diffusion (E_D) were calculated. In similar way, the activation energies for permeation of water (E_{pw}) and IPA (E_{pIPA}), and diffusion of water (E_{Dw}) were calculated (the plots are not given for reasons of space). The values thus obtained are presented in Table 1. From this Table, it is observed that the pure chitosan membrane (M) exhibits higher E_p and E_D values compared to those of the TGDMP incorporated membranes (M-1 to M-4). This indicates that both permeation and diffusion processes require more energy for transport of molecules through the pure chitosan membrane than the nanocomposite membranes. Obviously, the TGDMP incorporated membranes consumed significantly less energy because of increased hydrophilicity and decreased crystallinity. This has resulted in noticeable changes in the values from membrane M-1 to M-3 with increasing the amount of TGDMP. Although, E_p values are slightly higher than those of E_D values in all the membranes, the difference is insignificant, suggesting that both sorption and diffusion contribute equally to the PV process. The same trend is also observed for permeation and diffusion of water (E_{pw} and E_{Dw}). However, a significant difference was noticed between the apparent activation energy values for water (E_{pw}) and IPA (E_{pIPA}). This further suggests that membranes incorporated with higher amount of TGDMP demonstrated greater separation efficiency towards water. The E_p and E_D values ranged between 20.00 and 2.52, and 19.72 and 2.48 kJ/mol, respectively. Using these values, we have further calculated the heat of sorption as:

$$\Delta H_s = E_p - E_D \,. \tag{8}$$

The resulting ΔH_s values are included in Table 1. The ΔH_s values give additional information about the transport of molecules through the polymer matrix. It is a composite parameter involving the contributions of both Henry's and Langmuir's mode of sorption.[46] Henry's law states that the heat of sorption is positive for liquid transport, leading to the dissolution of chemical species into a site within the membrane, giving an endothermic contribution to the sorption process. However, Langmuir's sorption requires the pre-existence of a site in which sorption occurs by a hole filling mechanism, giving an exothermic contribution. The ΔH_s values obtained in the present study are positive, indicating that there is a good compatibility between TGDMP and the chitosan through electrostatic interactions and hydrogen bonding, as a result, Henry's mode of sorption becomes predominant, giving an endothermic contribution.

4. Conclusions

High-performance CS/TGDMP nanocomposite membranes were successfully prepared by a solution casting technique. An increase of TGDMP content in the membrane matrix results in a simultaneous increase of both permeation flux and separation factor. This was explained on the basis of significant enhancement of hydrophilicity and the establishment of hydrogen bonding and electrostatic interactions in the membrane matrix. The membrane containing 1.2 mass% of TGDMP shows the highest separation factor of 1,050 with a flux of 7.37×10^{-2} kg/m^{2}h at 30 ^{o}C for 10 mass% of water in the feed. Experimental data also reveal that the total flux and flux of water overlap with each other, particularly for TGDMP incorporated membranes, suggesting that the developed membranes are highly selective towards water and this is in agreement with the diffusion data. The membranes show significant lower activation energy values for water permeation (E_{pw}) than that of IPA permeation (E_{pIPA}), suggesting that TGDMP incorporated membranes have higher separation efficiency. The estimated E_p and E_D values ranged between 20.00 and 2.52, and 19.72 and 2.48 kJ/mol, respectively. The ΔH_s values obtained in the present study are positive, suggesting that Henry's mode of sorption is predominant.

Acknowledgements

This work was supported by the University Grants Commission (UGC), New Delhi (Grant No. 37-245/3009, SR). The authors thank the Department of Physics, Indian Institute of Science, Bangalore, for the use of the wide-angle X-ray diffraction facility.

Electronic supplementary information (ESI) available: Scheme for the synthesis of TGDMP, TGA curves, Tables of diffusion coefficients and temperature effect, Figures of Activation energy values.

References

1. Y. Huang, R. W. Baker and J. G. Wijmans, *Ind. Eng. Chem. Res.*, 2013, **52**, 1141–1149.
2. J. Zuo and T. S. Chung, *J. Mater. Chem. A*, 2013, **1**, 9814–9826.
3. A. J. Ragauskas, C. K. Williams, B. H. Davison, G. Britivsek, J. Cairney, C. A. Eckert, W. J. Frederick, J. P. Hallett, D. J. Leak, C. L. Liotta, J. R. Mielenz, R. Murphy, R. Templer and T. Tschaplinski, *Science*, 2006, **311**, 484–489.
4. C. Gao, M. Zhang, J. Ding, F. Pan, Z. Jiang, Y. Li and J. Zhao, *Carbohyd. Polym.*, 2014, **99**, 158–165.
5. Z. Dong, G. Liu, S. Liu, Z. Liu and W. Jin, *J. Membr. Sci.*, 2014, **450**, 38–47.
6. J. G. Varghese, R. S. Karuppannan and M. Y. Kariduraganavar, *J. Chem. Eng. Data*, 2010, **55**, 2084–2092.
7. G. Liu, D. Yang, Y. Zhu, J. Ma, M. Nie and Z. Jiang, *Chem. Eng. Sci.*, 2011, **66**, 4221–4228.
8. T. Zhu, Y. Luo, Y. Lin, Q. Li, P. Yu and M. Zeng, *Sep. and Purif. Technol.*, 2010, **74**, 242–252.
9. R. Srinivasan, IV, in *Green Materials for Sustainable Water Remediation and Treatment, RSC Green Chem.*, 2013, 51–81.
10. Q. G. Zhang, W. W. Hu, A. M. Zhu, and Q. L. Liu, *RSC Adv.*, 2013, **3**, 1855–1861**.**
11. F. Ding, H. Deng, Y. Du, X. Shi and Q. Wang, *Nanoscale*, 2014, **6**, 9477–9493.
12. A. M. Bonilla, M. L. Cerrada and M. F. García, (Eds.), II, in *Polymeric Materials with Antimicrobial Activity: From synthesis to applications*, *RSC*, 2014, 22–53.
13. Y. Wan, H. Wu, A. Yu and D. Wen, *Biomacromolecules*, 2006, **7**, 1362–1372.

14. S. K. Choudhari, A. A. Kittur, S. S. Kulkarni and M. Y. Kariduraganavar, *J. Membr. Sci*., 2007, **302**, 197–206.

15. S. Saber-Samandari, M. Gazi and O. Yilmaz, *Water Air Soil Pollut*., 2013, **224**, 1624–1635.

16. D. Hua, Y. K. Ong, Y. Wang, T. Yang, T. S. Chung, *J. Membr. Sci*., 2014, **453**, 155–167.

17. H. G. Premakshi, K. Ramesh and M. Y. Kariduraganavar, *Chem. Eng. Res. Des*., 2015, **94**, 32–43.

18. H. G. Premakshi, A. M. Sajjan, A. A. Kittur and M. Y. Kariduraganavar, *J. Appl. Polym. Sci.*, 2015, **132**, Issue 2.

19. F. Bellezza, A. Cipiciani, U. Costantino and M. E. Negozio, *Langmuir*, 2002, **18**, 8737–8742.

20. H. X. Wu, C. H. Liu, Y. J. Yang, J. G. Chen, P. R. Chang and Y. Chen, *Polym. Compos*., 2010, **31**, 1938–1946.

21. M. Casciola, G. Alberti, A. Ciarletta, A. Cruccolini, P. Piaggio and M. Pica, *Solid State Ionics*, 2005, **176**, 2985–2989.

22. Y. J. Yang, C. H. Liu, H. X. Wu and R. Li, *Carbohydr. Res*., 2010, **345**, 148–153.

23. T. Y. Tsai, Y. J. Wu and F. J. Hsu, *J. Phys. Chem. Solids*, 2008, **69**, 1379–1382.

24. R. Li, C. Liu, J. Ma, Y. Yang and H. Wu, *Polym. Bull*., 2011, **67**, 77–89.

25. P. S. Rachipudi, M. Y. Kariduraganavar, A. A. Kittur and A. M. Sajjan, *J. Membr. Sci*., 2011, **383**, 224–234.

26. A. M. Sajjan and M. Y. Kariduraganavar, *J. Membr. Sci*., 2013, **438**, 8–17.

27. E. Jaimez, G. B. Hix and R. C. T. Slade, *Solid State Ionics*, 1997, **97**, 195–201.

28. H. J. Warren, S. S. Hogarth, A. K. Muir, J. C. Whittaker, D. D. Costa, J. Drennan and G. Q. Lu, *Solid State Ionics*, 2007, **177**, 3389–3394.
29. P. Misaelides, S. Sarri, D. Zamboulis, G. Gallios, I. Zhuravlev and V. V. Strelko, *J. Radioanal Nucl. Chem*., 2006, **268**, 53–58.
30. R. Thakkar and U. *Chudasama, Electrochim. Acta*, 2009, **54**, 2720–2726.
31. K. Jia, B. C. Pan, Q. R. Zhang, W. M. Zhang, P. J. Jiang, C. H. Hong, B. J. Pan and Q. X. Zhang, *J. Colloid. Interface Sci*., 2008, **318**, 160–166.
32. I. Y. Kim, M. K. Yoo, B. C. Kim, S. K. Kim, H. C. Lee and C. S. Cho, *Int. J. Biol. Macromol*., 2006, **38**, 51–58.
33. J. T. Yeh, C. L. Chen and K. S. Hiang, *Mater. Lett*., 2007, **61**, 1292–1295.
34. S. F. Wang, L. Shen, W. D. Zhang and Y. J. Tong, *Biomacromolecules*, 2005, **6**, 3067–3072.
35. T. Zhu, Y. Luo, Y. Lin, Q. Li, P. Yu and M. Zeng, *Sep. and Purif. Technol*., 2010, **74**, 242–252.
36. G. Yang, L. N. Zhang, T. Peng and W. Zhong, *J. Membr. Sci*., 2000, **175**, 53–60.
37. M. H. Eikerling and P. Berg, *Soft Matter*, 2011, **7**, 5976–5990.
38. A. Vishnyakov and A. V. Neimark, *J. Phys. Chem. B*, 2001, **105**, 9586–9594.
39. Y. M. Lee, D. Bourgeois and G. Belfort, *J. Membr. Sci*., 1989, **44**, 161–181.
40. A. A. Kittur, M. Y. Kariduraganavar, U. S. Toti, K. Ramesh and T. M. Aminabhavi, *J. Appl. Polym. Sci*., 2003, **90**, 2441–2448.
41. J. G. Varghese, A. A. Kittur, P. S. Rachipudi and M. Y. Kariduraganavar, *J. Membr. Sci*., 2010, **364**, 111–121.

42. A. V. Yakovlev, M. G. Shalygin, S. M. Matson, V. S. Khotimskiy and V. V. Teplyakov, *J. Membr. Sci.*, 2013, **434**, 99–105.
43. A. Yamasaki, T. Iwatsubo, T. Masuoka and K. Mizoguchi, *J. Membr. Sci.*, 1994, **89**, 111–117.
44. S. P. Kusumocahyo and M. Sudoh, *J. Membr. Sci.*, 1999, **161**, 77–83.
45. R. Y. M. Huang and C. K. Yeom, *J. Membr. Sci.*, 1991, **58**, 33–47.
46. D. H. Weinkauf and D. R. Paul, in *Barrier Polymers and Structures*, W. J. Koros (Eds.), *ACS Symp. Ser.*, Washington, DC, 1990, **423**, 61–91.